Talanta 85 (2011) 1344–1349

Contents lists available at ScienceDirect

Talanta

journal homepage: www.elsevier.com/locate/talanta

An enzymeless organophosphate pesticide sensor using Au nanoparticle-decorated graphene hybrid nanosheet as solid-phase extraction

Jingming Gong*, Xingju Miao, Ting Zhou, Lizhi Zhang*

Key Laboratory of Pesticide & Chemical Biology of Ministry of Education, College of Chemistry, Central China Normal University, Wuhan 430079, PR China

ARTICLE INFO

Article history:
Received 28 January 2011
Received in revised form 7 June 2011
Accepted 9 June 2011
Available online 16 June 2011

Keywords:
Monodispersed Au nanoparticles
Graphene
Solid phase extraction (SPE)
Stripping voltammetric analysis
Methyl parathion

ABSTRACT

A sensitive enzymeless organophosphate pesticides (OPs) sensor is fabricated by using Au nanoparticles (AuNPs) decorated graphene nanosheets (GNs) modified glassy carbon electrode as solid phase extraction (SPE). Such a nanostructured composite film, combining the advantages of AuNPs with two dimensional GNs, dramatically facilitates the enrichment of nitroaromatic OPs onto the surface and realizes their stripping voltammetric detection of OPs by using methyl parathion (MP) as a model. The stripping voltammetric performances of captured MP were evaluated by cyclic voltammetric and square-wave voltammetric analysis. The combination of the nanoassembly of AuNPs-GNs, SPE, and stripping voltammetry provides a fast, simple, and sensitive electrochemical method for detecting nitroaromatic OPs. The stripping analysis is highly linear over the MP concentration ranges of 0.001–0.1and 0.2–1.0 μg mL^{-1} with a detection limit of 0.6 ng mL^{-1}. This designed enzymeless sensor exhibits good reproducibility and acceptable stability.

1. Introduction

In modern agriculture, extensive use of organophosphates pesticides (OPs) for pest control has raised serious public concern regarding the healthiness, environment and food safety [1–3]. They disrupt the cholinesterase enzyme that regulates acetylcholine (AChE), which often causes respiratory paralysis and death [4]. Undoubtedly, OP residues in crop, livestock, and water pose a severe threat to human life. For the sake of human health protection and environmental control, the detection of trace level of OPs has become increasingly important. Traditional analysis of OPs is routinely carried out by gas/liquid chromatography or mass spectroscopy [5–7]. These methods often require complicated pretreatment steps, extensive labor resources, and are not applicable for on-site determination. Over the past few years, enzyme-based inhibition/noninhibition biosensors, especially based on various electrochemical transducers, have emerged as a promising alternative to detect pesticides [2,3,8–16]. Nevertheless, the operational conditions are mostly limited by the denaturation of enzymes. To overcome this problem, a nonenzymatic sensor, stripping voltammetric analysis combined with solid phase extraction (SPE) of OPs appears to be an ideal and highly sensitive technology [17–20]. As well known, solid phase extraction (SPE) is a most popular method for sample preparation and separation [21,22]. For stripping analysis, the design of solid-phase extractor is a considerably critical issue, directly related with the stripping peak signal. In this regard, zirconia nanoparticles or hollow fibers [18,23], carbon paste [17], carbon nanotubes [24], molecularly imprinted polymer [25], and layered double hydroxides-based supramolecules [19], respectively, have been recognized as highly efficient SPE for the enrichment of OPs. Despite these outstanding achievements obtained, to meet the fast-developing detection requirements (*e.g.* high sensitivity, portable instruments, and simple operations), it is still a great challenge to construct a high-performance SPE platform for sensitive and selective detection of OPs.

Graphene nanosheet (GN), as a "rising star" material, a single layer of sp^2 hybridized carbon atoms packed into a dense honeycomb two-dimensional (2D) sheet, has attracted tremendous attention since experimentally produced in 2004 [26–28]. Due to its novel properties, such as high surface areas (calculated value, 2630 m^2/g), exceptional thermal and mechanical properties, and high electrical conductivity, GN provides potential applications in synthesizing nanocomposites, nanoelectronics, electromechanical resonators, and ultrasensitive sensors [29–32]. Rafiee et al. [33] reported that the planar geometry of graphene sheets, compared with the tube-shaped carbon nanotubes, could be in more close contact with the surrounding matrix. Furthermore, the "wrinkly" surfaces of graphene could interlock well with the exotic assembly or the adsorbed targets [34]. This feature provides a new avenue for utilizing graphene-based hybrid composite as a multifunctional nanoassembly system. Metal

* Corresponding authors. Tel.: +86 27 6786 7535.
E-mail addresses: jmgong@mail.ccnu.edu.cn (J. Gong), zhanglz@mail.ccnu.edu.cn (L. Zhang).

0039-9140/$ – see front matter © 2011 Elsevier B.V. All rights reserved.
doi:10.1016/j.talanta.2011.06.016

nanoparticles (NPs), owing to their unique properties, assembled on various supporting skeleton as sensing platform have been extensively utilized in analytical electrochemistry [35–37]. The nanocomposite of 2D GNs combined with 0D metal (*e.g.*, Au, Pd, Pt) NPs, have also been highly concerned recently for constructing electrochemical sensors, such as electrochemical determination of glucose [38,39], β-nicotinamide adenine dinucleotide [40], dopamine [41], cytochrome c [42], DNA [39] and heavy metal ions (Hg^{2+}) [43], etc. Obviously, graphene-based materials (metal NPs-graphene nanocomposite) show obvious superiorities on sensing applications. However, to the best of our knowledge, there is no report on the determination of OPs by using graphene-based nanocomposite as SPE to develop enzymeless OPs sensor.

In this work, we describe an electrochemical stripping analysis of nitroaromatic OPs based on Au nanoparticles-decorated graphene hybrid nanosheets (AuNPs-GNs) as SPE. Uniform AuNPs were homogenously distributed onto the graphene nanosheet matrix, constructing a powerful sensing platform. The resulting nanocomposite combines the advantages of AuNPs (extraordinarily catalytic activity, good conductivity) together with the graphene nanosheets. Furthermore, as a supporting skeleton, graphene nanosheets not only have enlarged active surface area, high electrical conductivity, and unique interlock effect toward the target, but also posses rich π-electron in the basal plane (C_π sites), which would have strong affinity for nitroaromatic OPs through strong π–π interactions. It is expected to dramatically facilitate the enrichment of OPs and realize their rapid, stable and sensitive stripping voltammetric detection. Encouragingly, the combination of SPE, the nanoassembly of AuNPs-2D GNs, and stripping voltammetry may open up new opportunities for fast, simple and sensitive analysis of OPs.

2. Experiments

2.1. Reagents

Methyl parathion (MP) was obtained from Treechem Co. (Shanghai, China). Chitosan from crab shells (85% deacetylated) was purchased from Sigma. Chitosan solution was prepared by adding chitosan flakes into water, gradually dropping HCl solution to the mixture to maintain the pH near 5 and then removing the undissolved part by a 0.45-μm syringe filter unit. The final concentration of chitosan solution was estimated to be 0.03 mg mL^{-1}. Polyvinylpyrrolidone (PVP) was obtained from Sinopharm Medicine Holding Co. (Shanghai, China). Ammonia solution (28 wt%) was purchased from Aladdin Co. (Shanghai, China). $KAuCl_4$ was obtained from Alfa Aesar. All other chemicals were of analytical-reagent grade and used without further purification. Doubly distilled water was used. The 0.1 M phosphate buffer solutions (PBS) of different pH values were prepared for use.

2.2. Apparatus

Electrochemical measurements were performed on a CHI 660C electrochemical workstation (CHI, USA) with a conventional three-electrode system comprising a platinum wire as an auxiliary electrode, a saturated calomel electrode (SCE) as reference, and the modified or unmodified glass carbon electrode (GCE) as a working electrode. The general morphology of the products was characterized by the scanning electron microscopy (SEM, JSM-5600). Tapping-mode atom force microscopy (AFM) was conducted with a DI Nanoscope (Veeco Instruments, Inc., USA). All experiments were carried out at ambient temperature.

2.3. Electrode preparation

Prior to modification, the basal GCE was polished to a mirror finish using 1.0, 0.3 and 0.05 μm alumina slurries. After each polishing, the electrode was sonicated in ethanol and doubly distilled water for 5 min, successively, in order to remove any adsorbed substances on the electrode surface. Finally, it was dried under nitrogen atmosphere ready for use.

Graphite oxide was synthesized from graphite by a modified Hummers method [44,45]. PVP-protected graphene was prepared by a modified method according to the literature [38]. Because graphene sheets tend to form irreversible agglomerates or even restack to graphite through strong π–π stacking and van der Waals interaction [28], it is difficult for graphene to be directly dispersed into solvents to form a uniform dispersion. This brings about the difficulty for the construction of electrochemical sensing platforms. Here, chitosan was selected as a stabilizer to disperse graphene into an aqueous solution. Due to its excellent capability for film formation, nontoxicity, biocompatibility, mechanical strength, and good water permeability, chitosan is commonly used to disperse nanomaterials and immobilize enzymes for constructing biosensors [46–48]. A certain amount of PVP-protected graphene was dispersed into 0.5 mL of 0.03 mg mL^{-1} chitosan to form a homogenous dispersion under mild ultrasonication for 2 h. 10 μL of the resulting chi-graphene dispersion was dropped onto the surface of the cleaned GCE and was kept at room temperature till dry (labeled as chi-GNs/GCE). The further modification of AuNPs onto chi-GNs/GCE was conducted by CV scanning from 0.2 to 1.0 V in 0.1 M KCl solution containing 2 mM $KAuCl_4$ at a scan rate of 50 mV/s for 7 cycles. After modification, the electrode (denoted as AuNPs-chi-GNs/GCE) was thoroughly rinsed with water and kept at room temperature for further use.

2.4. Measurement procedure

The AuNPs-chi-GNs-modified GCE was first immersed into a stirred sample solution containing the desired MP concentration for a given time, and rinsed with water. Then, it was transferred into the blank electrolyte (0.1 M, pH 5.7 PBS) for SWV measurements. Multiple successive SWV scanning was used to remove the bound MP until the anodic stripping response disappeared. Also, it made the regeneration of the sensor surface. Before electrochemical measurements, the electrolyte solution was purged with nitrogen gas for 10 min.

3. Results and discussion

3.1. Characterization of the modified electrode surface

Typical SEM image of the as-synthesized graphene powder shows 2D nanosheet morphologies (Fig. 1A), exhibiting a few thin wrinkles onto the surface. From the atomic force microscopy (AFM) image, the thickness of most GNs was less than 1.0 nm (Fig. 1B), consistent with the thickness of an individual graphene layer. With the successive deposition onto chi-GNs/GCE, uniform AuNPs of ~30 nm in average diameter formed randomly on the sheet (Fig. 1C). Obviously, the generated AuNPs were homogenously distributed onto the graphene nanosheet matrix, constructing a monodispersed AuNPs-decorated graphene hybrid nanosheet assembly.

3.2. Electrochemical reactivity

The capability of electron transfer of different electrodes was investigated by electrochemical impedance spectra (EIS), shown in Fig. 2. It can be seen that EIS of the bare GCE is composed of a semicircle and a straight line featuring a diffusion-limiting

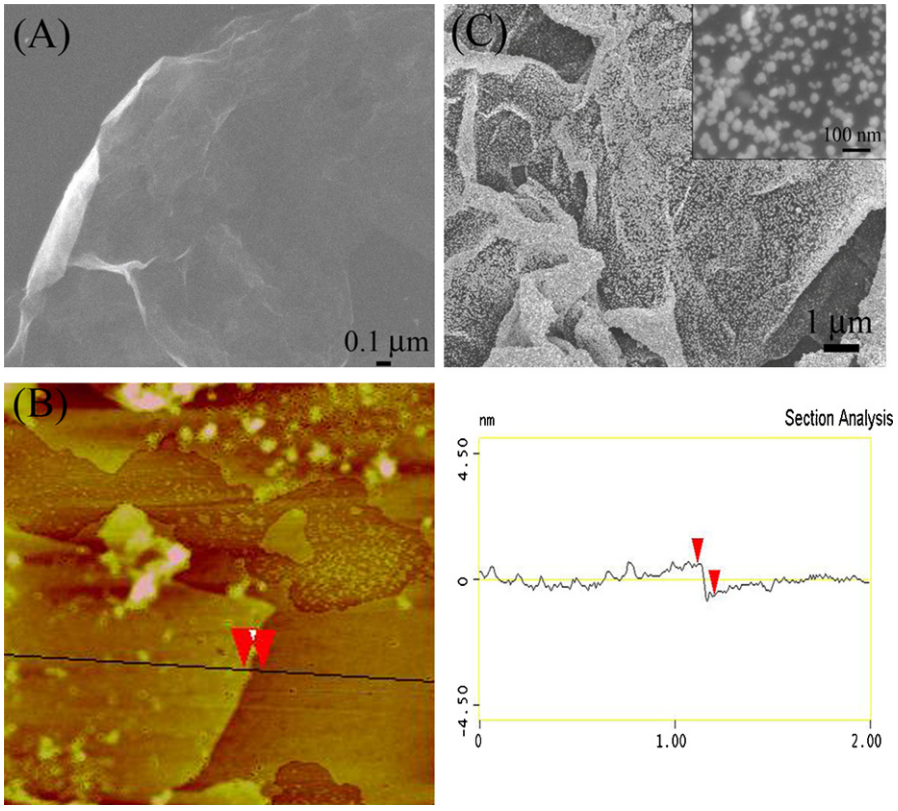

Fig. 1. Typical SEM images of the as-synthesized chi-graphene (A); AuNPs-coated chi-graphene/GCE (B); typical AFM image of the as-prepared chi-graphene nanosheet on mica and its section analysis (C).

step of the $Fe(CN)_6^{4-/3-}$ processes (curve a). With the modification of graphene onto GCE, the diameter of the semicircle decreased. It shows the consistency with the fact that graphene possesses high electrical conductivity with deceased charge transfer resistance (R_{ct}). Compared with the EIS of the bare GCE, the diameter of the semicircles was successively decreased in the order from chi-GNs/GCE (curve b) to AuNPs-chi-GNs/GCE (curve c), indicating the increasingly facile heterogeneous electron transfer kinetics. This demonstrates that the electrochemical activity of AuNPs-chi-GNs/GCE is higher than that of chi-GNs/GC and GC electrodes.

The cyclic voltammetric experiments were further carried out by using $Fe(CN)_6^{3-}$ as the electrochemical probe. CV curves of GC modified with different materials (inset of Fig. 2) show consistence with EIS results. It can be seen that $Fe(CN)_6^{4-/3-}$ redox reaction at the bare GCE gave a couple of well-behaved CV peaks at E_m of 0.210 with ΔE_p of 65 mV. With the modification of graphene (chi-GNs/GCE), and the further decoration of AuNPs (AuNPs-chi-GNs/GCE), respectively, the peak currents were increased apparently with ΔE_p decreased successively. Moreover, a great enhancement of the background current was observed at AuNPs-chi-GNs/GCE, assigned to enlarged surface areas. Obviously, the modification of AuNPs-chi-GNs onto GCE greatly enhances the active area of the surface, providing an advantageous and high-performance platform for sensing applications.

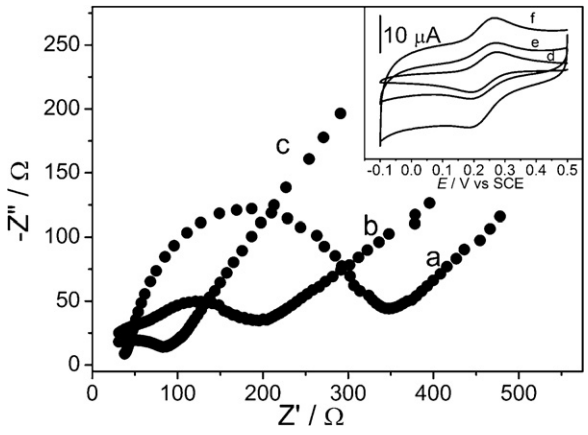

Fig. 2. Nyquist plots obtained at GC electrode (a), chi-GN/GCE (b), and AuNPs-chi-GN/GCE (c) in 10 mM $Fe(CN)_6^{3-/4-}$ containing 0.1 M KCl. The frequency range is from 1 Hz to 100 kHz. Inset: cyclic voltammograms of 10 mM $Fe(CN)_6^{3-/4-}$ at GC electrode (d), chi-GN/GCE (e), and AuNPs-chi-GN/GCE (f) in 0.1 M KCl.

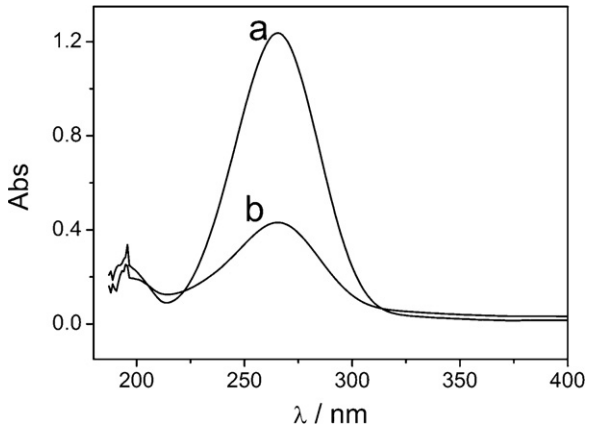

Fig. 3. UV–vis spectra of MP solution before SPE (a) and after SPE (b). MP concentration before SPE: 1.0 μg mL^{-1}; extraction time: 20 min.

3.3. UV–vis spectra

To prove that AuNPs-decorated graphene nanoassembly can be used for SPE of methyl parathion, UV–vis spectra of MP solution before (curve a) and after SPE (curve b) were shown in Fig. 3. The freshly prepared MP solution (1.0 μg mL^{-1}) showed a maximum absorbance (λ_{max}) at 265 nm, which was the characteristic absorbance peak of methyl parathion solution [49]. After the AuNPs-chi-GNs/GCE was immersed in the methyl parathion solution for ~20 min, the absorbance showed a great decrease, indicating the decrease of the amount of methyl parathion in solution due to the strong SPE ability of the present nanoassembly toward methyl parathion, while no obvious change of the absorbance was observed when a pretreated GCE without AuNPs-GNs layer was immersed in the solution. The phenomenon confirmed that AuNPs-decorated graphene hybrid nanosheet assembly provides an efficient platform as the host of nitroaromatic OPs, it provides a facile approach to attach OPs onto an electrode surface.

3.4. Effect of methyl parathion on response of AuNPs-chi-GNs/GCE

Fig. 4 displays the CV of MP captured on AuNPs-chi-GNs/GCE in 0.1 M PBS (pH 5.7). During the potential range from −0.8 to 0.5 V, no obvious redox peak appeared in the absence of MP (curve a). However, a pair of well-defined redox peaks (E_{pa}, −0.01 V; E_{pc}, −0.07 V) and an irreversible reduction peak (E_{pc}, −0.57 V) were observed (curve b) with the capture of MP onto AuNPs-chi-GNs/GCE. The irreversible reduction peak corresponds to the reduction of the nitro group to the hydroxylamine group (reaction (1)). The reversible redox peaks are attributed to a two-electron-transfer process (reactions (2) and (3)), shown as below. These profiles are consistent with those described elsewhere for nitroaromatic OPs [17–20].

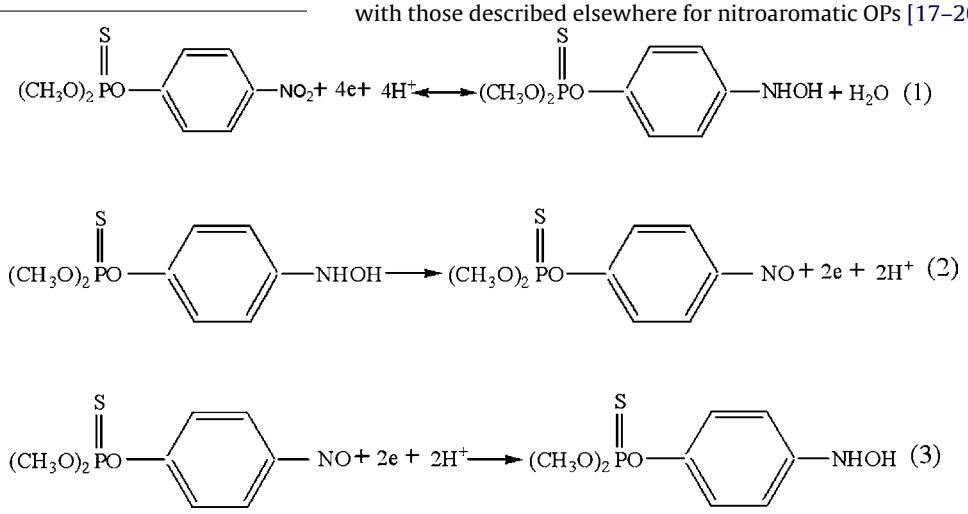

SWV analysis has a higher sensitivity than that of other electrochemical techniques. As shown in the inset of Fig. 4, no anodic stripping peak was observed at AuNPs-chi-GNs/GCE in blank PBS (curve a). Evidently, a very sharp and well-defined stripping peak at a potential of about 0.056 V vs. SCE (curve c) appeared with the capture of MP into the nanoassembly. Compared with the direct measurement in MP sample solution (curve b), the stripping peak current at MP captured AuNPs-chi-GNs/GCE was greatly enhanced. This may be attributed to the enlarged surface area, the enhanced electron transfer, the strong π–π interactions and the unique interlock effect of graphene toward the target of MP. Obviously, the presence of an AuNPs-chi-GNs film plays a great role, providing an advantageous platform for the preconcentration of MP. The SPE through the capture of MP into the nanoassembly of AuNPs-chi-GNs, leads to the enrichment of MP onto the surface of the electrode, and is therefore responsible for the significant enhancement of the current response.

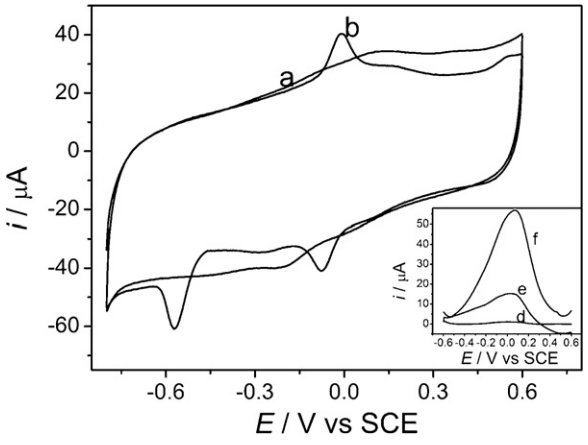

Fig. 4. Cyclic voltammograms of AuNPs-chi-GN/GCE (a), MP captured onto AuNPs-chi-GN/GCE (b) in 0.1 M PBS (pH 5.7). Scan rate: 100 mV/s. Inset: stripping voltammograms obtained at AuNPs-chi-GN/GCE in the absence of MP (c), the solution containing 0.2 μg mL^{-1} MP without preconcentration (d), and after SPE in 0.2 μg mL^{-1} MP (e). SWV conditions: scanning potential range, −0.4 to 0.3 V; frequency, 25 Hz; potential increment, 4 mV; amplitude of the square-wave, 20 mV. Electrolyte: 0.1 M PBS pH 5.7.

3.5. Optimization for the detection of MP at AuNPs-chi-GNs/GCE

We further optimized the experimental parameters to get high-performance stripping analysis of OPs. First, as the supporting skeleton, the amount of graphene dispersed onto GCE sharply influenced the electrochemical response. With casting the different dispersion concentration of graphene onto GCE, the final stripping response of MP at AuNP-chi-GNs modified GCE rose at first up to 0.40 mg mL^{-1} and then decreased at higher concentration (Fig. 5A). In other word, when the concentration of graphene was 0.4 mg mL^{-1}, the stripping peak current of MP was best.

Since the AuNPs-based ensemble plays an important role in the performance of sensors, the influence of the amount of monodispersed AuNPs onto the sheet was investigated by controlling the cycles of CV scanning (in 2 mM $KAuCl_4$ + 0.1 M KCl). The potential scanning cycles would directly affect the size distribution of AuNPs. As shown in Fig. 5B, with the potential scanning cycles increased, the stripping peak current of MP rose at first up to 7 cycles and then decreased. It is likely related to the nanostructural platform ensembled by AuNPs-chi-GNs onto the electrode. The enhanced surface area from the modification of metal NPs enables more avail-

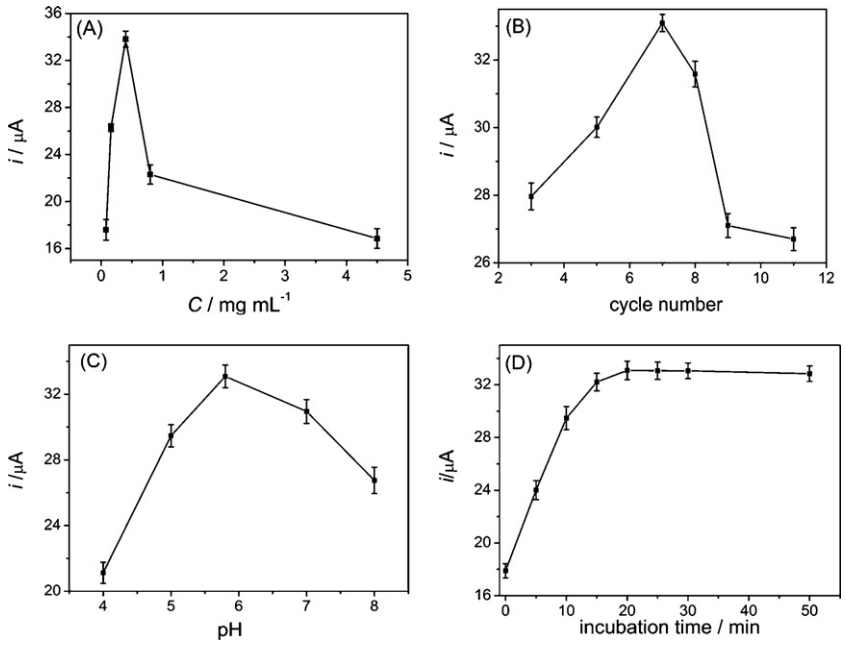

Fig. 5. Effects of the amount of chi-graphene precasted onto the substrate (A), the potential scanning cycles in 2 mM $KAuCl_4$ + 0.1 M KCl (B), the pH of adsorption medium (C), and the extraction time (D) toward the adsorption of MP onto AuNPs-chi-GN/GCE. SWV conditions are the same to those in Fig. 4.

able active sites on the electrode surface for MP capture. While the potential scanning cycles were further increased, the metal NPs would be continuously generated, even coalesced and finally aggregated, resulting in the decreased sensing performance. Thus, the condition of 7 potential cycles was optimal for the preparation of AuNPs-chi-GNs modified GCE.

The response of MP was also dependent on pH of adsorption media. The stripping signal was enhanced with an increase of pH up to 5.7, but decreased at higher pH (Fig. 5C). Since basic media would result in the degradation of OP compounds and H^+ was involved in the irreversible reduction of MP, a pH value of 5.7 was selected for measurements in this study [50].

It was found that extraction time was another one of the most influential parameters in pesticide analysis. The peak currents increased rapidly with an increase of immersion time, and then tended to be stable at ~20 min. This indicates that the uptake of MP into the nanoassembly reaches saturation (Fig. 5D).

3.6. Analytical performance for the detection of methyl parathion

Fig. 6 displays the SWV response of adsorbed MP by the SPE process at AuNPs-chi-GNs/GCE. Well-defined peaks, proportional to the concentration of the corresponding MP, were observed in two ranges, 0.001–0.1 and 0.2–1.0 μg mL^{-1}. The linearization equations were $i/\mu A = 16.81 + 256.3c/\mu g\,mL^{-1}$, and $i/\mu A = 47.61 + 11.17c/\mu g\,mL^{-1}$, with the correlation coefficients of 0.9908 and 0.9987, respectively (inset of Fig. 6). At relatively low concentrations of the analyte, the outer more accessible active surface area could be fully covered with a lower competition for the surface. It ensures a more efficient uptake of methyl parathion, leading to a higher sensitivity for the lower concentrations. Therefore, two linear ranges with a "switch" in slope appeared. The similar results have ever been reported in other systems [51,52]. A detection limit of 0.6 ng mL^{-1} was obtained with the calculation based on signal-noise ratio equal to 3. It is significantly lower than 13.2 ng mL^{-1} at a carbon-paste electrode by using stripping analysis [17,18], lower than those reported with enzyme-based inhibitor electrochemical sensors [13–15,19], and comparable with those obtained using ZrO_2 or LDHs-based SPE [17–20]. Our results demonstrated that the proposed AuNPs-chi-GNs composite film was reliable for the determination of OPs. The relative standard deviation was 5.6% for 10 replicate determinations of 0.1 μg mL^{-1} MP, indicating acceptable reproducibility.

The stability of the AuNPs-chi-GNs modified electrode could be maintained by being stored at 4 °C in a dry condition. No obvious decrease in the response of MP was observed in the first 10-day storage. After a 30-day storage period, the sensor retained 86% of its initial current response. Interferences arising from other electroactive nitrophenyl derivatives such as p-nitrophenol, nitrobenzene, p-nitroaniline, trinitrotoluene (TNT) and other oxygen-containing inorganic ions (PO_4^{3-}, SO_4^{2-}, NO_3^-) were used to evaluate the selectivity of the AuNPs-chi-GNs/GCE to MP. As shown in Fig. 7, one can see that no obvious interferences were observed with the peak currents of MP varied slightly. It is likely due to the strong π–π interaction between the nanoassembly of AuNPs decorated GNs and nitroaromatic OPs. Also, such a low stripping potential of

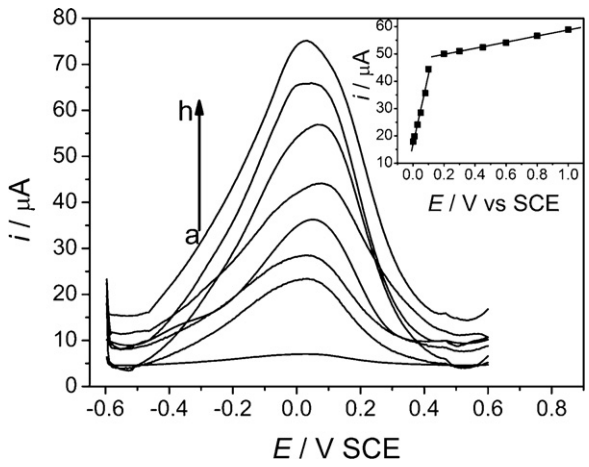

Fig. 6. Stripping voltammograms of increasing MP concentrations (from bottom to top, 0, 1, 10, 30, 80, 200, 600, and 1000 ng mL^{-1}, respectively). The inset shows the calibration curve. Electrochemical stripping detection conditions are the same to those in Fig. 4.

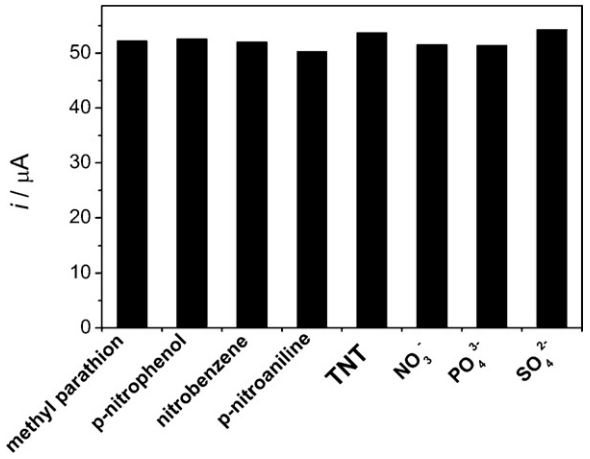

Fig. 7. Stripping signals of 200 ng mL^{-1} MP in the absence and presence of 2 μg mL^{-1} p-nitrophenol, 2 μg mL^{-1} nitrobenzene, 2 μg mL^{-1} p-nitroaniline, 2 μg mL^{-1} trinitrotoluene, 0.4 mM PO_4^{3-}, 0.4 mM SO_4^{2-}, and 0.4 mM NO_3^-, respectively. Electrochemical stripping detection conditions are the same to those in Fig. 4.

0.056 V applied could avoid the interference efficiently since the oxidation potentials of those phenol compounds are more than 0.3 V.

To further demonstrate the practicality of the present electrode, it was evaluated by processing real samples. We performed the recovery tests by adding different amounts of MP into real samples, including garlic, cabbage and tea. Results are summarized as Table S1. The original MP concentration in the cabbage sample was tested to be 5.86 ng mL^{-1}, while the original MP in the tea sample was 6.17 ng mL^{-1}. The recoveries of the spiked MP are from 96.2% to 105.0% for the real samples. The results indicate that the proposed method is highly accurate, precise and reproducible. It can be used for direct analysis of relevant samples.

4. Conclusions

This work has successfully demonstrated a simple and efficient strategy for stripping analysis of OPs at AuNPs-chi-GNs modified GCE. Monodispersed AuNPs are homogenously distributed onto 2D graphene nanosheet matrix, constructing a nanoassembly of AuNPs-decorated 2D graphene hybrid nanosheets. The as-prepared composite matrix, combining the advantages of graphene nanosheets together with AuNPs, greatly facilitated the preconcentration of MP onto the surface with the stripping current response greatly enhanced. The resulting biosensor showed both good reproducibility and ideal stability. This work has expanded the scope of the metal NPs-graphene nanocomposite material to the field of electroanalytical chemistry, and holds great promise for the routing sensing and biosensing applications. We believe that the combination of the nanoassembly of AuNPs-2D GNs and SPE as well as SWV will pave the new way for electrochemical detection of OPs.

Acknowledgements

This work was supported by National Science Foundation of China (Grant 20803026), Self-determined Research Funds of CCNU from the Colleges' Basic Research and Operation of MOE (Grant CCNU10A01006), and Program for Innovation Team of Hubei Province (Grant 2009CDA048).

Appendix A. Supplementary data

Supplementary data associated with this article can be found, in the online version, at doi:10.1016/j.talanta.2011.06.016.

References

[1] F. Arduini, F. Ricci, C.S. Tuta, D. Moscone, A. Amine, G. Palleschi, Anal. Chim. Acta 580 (2006) 155.
[2] B.X. Li, Y.Z. He, C.L. Xu, Talanta 72 (2007) 223–230.
[3] X.H. Li, Z.H. Xie, H. Min, Y.Z. Xian, L.T. Jin, Electroanalysis 24 (2007) 2551–2557.
[4] T.H. Kim, K. Kuca, D. Jun, Y.K. Jung, Bioorg. Med. Chem. Lett. 15 (2005) 2914–2917.
[5] P.S. Chen, S.D. Huang, Talanta 69 (2006) 669–675.
[6] L. Rotiroti, L.D. Stefano, I. Rendina, L. Moretti, Biosens. Bioelectron. 20 (2005) 2136–2139.
[7] C.C. Leandro, P. Hancock, R.J. Fussell, B.J. Keely, J. Chromatogr. A 1103 (2006) 94–101.
[8] A. Vakurov, C.E. Simpson, C.L. Daly, T.D. Gibson, P.A. Millner, Biosens. Bioelectron. 20 (2004) 1118–1125.
[9] S. Sotiropoulou, D. Fournier, N.A. Chaniotakis, Biosens. Bioelectron. 20 (2005) 2347–2352.
[10] G. Jeanty, J.L. Marty, Biosens. Bioelectron. 13 (1998) 213–218.
[11] O. Sadik, W. Land, J. Wang, Electroanalysis 15 (2003) 1149–1159.
[12] A. Mulchandani, P. Mulchandani, I. Kaneva, W. Chen, Anal. Chem. 70 (1998) 4140–4145.
[13] H. Schulze, S. Vorlovīa, F. Villatte, T.T. Bachmann, R.D. Schmid, Biosens. Bioelectron. 18 (2003) 201–209.
[14] F.N. Kok, V. Hasirci, Biosens. Bioelectron. 19 (2004) 665.
[15] G.D. Liu, Y.H. Lin, Anal. Chem. 78 (2006) 835–843.
[16] J.M. Gong, L.Y. Wang, L.Z. Zhang, Biosens. Bioelectron. 24 (2009) 2285–2288.
[17] G.D. Liu, Y.H. Lin, Electrochem. Commun. 7 (2005) 339–343.
[18] G.D. Liu, Y.H. Lin, Anal. Chem. 77 (2005) 5894–5901.
[19] J.M. Gong, L.Y. Wang, D.D. Song, L.Z. Zhang, Biosens. Bioelectron. 24 (2009) 2285–2288.
[20] J.M. Gong, L.Y. Wang, X.J. Miao, L.Z. Zhang, Electrochem. Commun. 12 (2010) 1658–1661.
[21] M.C. Hennion, J. Chromatogr. A 855 (2000) 73–75.
[22] L.H. Shi, X.Q. Liu, H.J. Li, W.X. Niu, G.B. Xu, Anal. Chem. 78 (2006) 1345–1348.
[23] L. Xu, H.K. Lee, Anal. Chem. 79 (2007) 5241–5248.
[24] C. Basheer, A.A. Alnedhary, B.S.M. Rao, S. Valliyaveettil, H.K. Lee, Anal. Chem. 78 (2006) 2853–2858.
[25] E. Turiel, A.M. Esteban, P. Fernández, C.P. Conde, C. Cámara, Anal. Chem. 73 (2001) 5133–5141.
[26] M.J. Allen, V.C. Tun, R.B. Kaner, Chem. Rev. 110 (2010) 132–145.
[27] K.S. Novoselov, A.K. Geim, S.V. Morozov, D. Jiang, Y. Zhang, S.V. Dubonos, I.V. Grigorieva, A.A. Firsov, Science 306 (2004) 666–669.
[28] D. Li, M.B. Muller, S. Gilje, R.B. Kaner, G.G. Wallace, Nat. Nanotechnol. 3 (2008) 101–105.
[29] J.D. Fowler, J.M. Allen, V.C. Tung, Y. Yang, B.H. Weiller, ACS Nano 3 (2009) 301–306.
[30] J.T. Robinson, F.K. Perkins, E.S. Snow, Z.Q. Wei, P.E. Sheehan, Nano Lett. 8 (2008) 3137–3140.
[31] N. Mohanty, V. Berry, Nano Lett. 8 (2008) 4469–4476.
[32] Y. Wang, Y.Y. Shao, D.W. Matson, J.H. Li, Y.H. Lin, ACS Nano 4 (4) (2010) 1790–1798.
[33] M.A. Rafiee, J. Rafiee, Z. Wang, H. Song, Z.Z. Yu, N. Koratkar, ACS Nano 3 (2009) 3884–3890.
[34] M.A. Rafiee, J. Rafiee, I. Srivastava, Z. Wang, H. Song, Z.Z. Yu, N. Koratkar, Small 6 (2010) 179–183.
[35] I. Willner, R. Baron, B. Willner, Adv. Mater. 18 (2006) 1109–1120.
[36] J. Lu, I. Do, L.T. Drzal, R.M. Worden, I. Lee, ACS Nano 2 (2008) 1825–1832.
[37] J.M. Gong, T. Zhou, D.D. Song, L.Z. Zhang, X.L. Hu, Anal. Chem. 82 (2010) 567–573.
[38] C.S. Shan, H.F. Yang, J.F. Song, D.X. Han, A. Ivaska, L. Niu, Anal. Chem. 81 (2009) 2378–2382.
[39] C.S. Shan, H.F. Yang, D.X. Han, Q.X. Zhang, A. Ivaska, L. Niu, Biosens. Bioelectron. 25 (2010) 1070–1074.
[40] W.J. Lin, C.S. Liao, J.H. Jhang, Y.C. Tsai, Electrochem. Commun. 11 (2009) 2153–2156.
[41] Y. Wang, Y. Li, L. Tang, J. Lu, J. Li, Electrochem. Commun. 11 (2009) 889–892.
[42] J.F. Wu, M.Q. Xu, G.C. Zhao, Electrochem. Commun. 12 (2010) 175–177.
[43] J.M. Gong, T. Zhou, D.D. Song, L.Z. Zhang, Sens. Actuators B 150 (2010) 491–497.
[44] W. Hummers, J. Offeman, J. Am. Chem. Soc. 80 (1958) 1339.
[45] N.I. Kovtyukhova, P.J. Ollivier, B.R. Martin, T.E. Mallouk, S.A. Chizhid, E.V. Buzaneva, A.D. Gorchinskiy, Chem. Mater. 11 (1999) 771–778.
[46] J.M. Gong, T. Liu, D.D. Song, X.B. Zhang, L.Z. Zhang, Electrochem. Commun. 11 (2009) 1873–1876.
[47] J.M. Gong, X.L. Hu, K.W. Wong, Z. Zheng, L. Yang, W.M. Lau, R.X. Du, Adv. Mater. 20 (2008) 2111–2115.
[48] J.M. Gong, L.Y. Wang, K. Zhao, D.D. Song, Electrochem. Commun. 10 (2008) 123–126.
[49] J. Wang, W. Sun, Z.H. Zhang, X.D. Zhang, R.H. Li, T. Ma, P. Zhang, Y. Li, J. Mol. Catal. A: Chem. 272 (2007) 84–90.
[50] J. Wang, M.P. Chatrathi, A. Mulchandani, W. Chen, Anal. Chem. 73 (2001) 1804–1808.
[51] O. Abollino, A. Giacomino, M. Malandrino, G. Piscionieri, E. Mentasti, Electroanalysis 20 (1) (2008) 75–83.
[52] L. Rassaei, M. Sillanpää, R.W. French, R.W. Compton, F. Marken, Electroanalysis 20 (12) (2008) 1286–1292.